reached by the ground state $\mathcal{W}$. In Fig. 5 (top), successive images, ~30 s apart, of the same vesicle indicate that it exhibits clear changes in shape. This sequence is compared with the numerically equilibrated surfaces within the $\mathcal{W}$ family shown in Fig. 5 (bottom), all of which have the same geometrical parameters $(v,\Delta a)$ and of course the same minimal energy. The very long time scale of the observed deformation mode demonstrates that this is not a thermally excited bending mode, the time scale for which is typically less than a second (*16*). We conclude that this deformation is a zero-energy mode and thus is experimental evidence of conformal diffusion. We have generalized these observations to genus 3 vesicles, although the description of conformal diffusion for these vesicles is much more delicate.

REFERENCES AND NOTES

1. For a review, see R. Lipowsky, *Nature* **349**, 475 (1991).
2. P. B. Canham, *J. Theor. Biol.* **26**, 61 (1970); W. Helfrich, *Z. Naturforsch. Teil C Biochem. Biophys. Biol. Virol.* **28**, 693 (1973); E. A. Evans, *Biophys. J.* **14**, 923 (1974).
3. The value of the elastic modulus is $\kappa \approx 10$ to $20k_BT \approx 10^{-12}$ erg for most phospholipids (where k_B is the Boltzmann constant and T is temperature). It is very small but nonetheless many times greater than the thermal energy scale ($k_BT/2$), which represents the energy attributed to each degree of freedom by thermal excitation. This explains why vesicles spontaneously fluctuate but do so within limits that enable the definition of stable shapes.
4. H. J. Deuling and W. Helfrich, *J. Phys. (Paris)* **37**, 1335 (1976).
5. L. Miao, B. Fourcade, M. Rao, M. Wortis, R. K. P. Zia, *Phys. Rev. A* **43**, 6843 (1991); U. Seifert, K. Berndl, R. Lipowsky, *ibid.* **44**, 1182 (1991); J. Käs and E. Sackmann, *Biophys. J.* **60**, 825 (1991); ———, R. Podgornik, S. Svetina, B. Zeks, *J. Phys. II (Paris)* **3**, 631 (1993).
6. The two models, as well as a third that combines both of them, have the same sets of shapes as equilibrium solutions. They differ in the elastic curvature energy attributed to each surface and thus in their definition of the most stable shape for a given set of geometrical constraints. This has consequences in the prediction of shape changes, induced, for example, by temperature changes (*5*). The models also differ in their definition of the relevant physical characteristics of the vesicles; in one, the asymmetry of the membrane is described by the area difference constraint,

$$\Delta A = D\int\int\left(\frac{1}{R_1}+\frac{1}{R_2}\right)dS \qquad (2)$$

where D is the bilayer thickness, and in the other by a spontaneous curvature, considered as a physicochemical characteristic.
7. F. Jülicher, U. Seifert, R. Lipowsky, *Phys. Rev. Lett.* **71**, 452 (1993).
8. By a proper rescaling of the vesicle, the area constraint can be eliminated and the number of physical constraints relevant to the determination of its shape can thus be reduced by one. Hence, we may consider only rescaled constraints such as the reduced volume $v = 6\sqrt{\pi}V/A^{3/2}$ and the reduced area difference $\Delta a = \Delta A/4\sqrt{\pi}D\sqrt{A}$, where V is the volume, A is the area of the surface, D is the thickness of the membrane, and ΔA is the area difference between the layers of the membrane. With these definitions, for a spherical vesicle, $v = 1$ and $\Delta a = 1$.
9. The image M' of any point M of the shape obtained by sphere inversion is defined by

$$\mathbf{OM}' = \frac{\mathbf{OM}}{\mathbf{OM}^2} \qquad (3)$$

where O is the inversion center.
10. T. J. Willmore, *Total Curvature in Riemannian Geometry* (Horwood, New York, 1982).
11. Z.-C. Ou-Yang, *Phys. Rev. A* **41**, 4517 (1990); U. Seifert, *Phys. Rev. Lett.* **66**, 2406 (1991); Z.-C. Ou-Yang, *Phys. Rev. E* **47**, 747 (1993); B. Fourcade, *J. Phys. II (Paris)* **2**, 1705 (1992); F. Jülicher, U. Seifert, R. Lipowsky, *ibid.* **3**, 1681 (1993).
12. M. Mutz and D. Bensimon, *Phys. Rev. A* **43**, 4525 (1991); B. Fourcade, M. Mutz, D. Bensimon, *Phys. Rev. Lett.* **68**, 2251 (1992); X. Michalet and D. Bensimon, *J. Phys. II (Paris)* **5**, 263 (1995); X. Michalet, thesis (Université Paris VII, Denis Diderot, 1994).
13. L. Hsu, R. Kusner, J. Sullivan, *Exp. Math.* **1**, 191 (1992); R. Kusner, *Pac. J. Math.* **138**, 317 (1989); H. B. Lawson Jr., *Ann. Math.* **92**, 335 (1970).
14. The three parameters are related to the position of the inversion center, which is defined by three spatial coordinates. In the spherical case, because of the high symmetry of the sphere, all positions are equivalent. In the toroidal case, because of the symmetry axis, nonequivalent positions differ only in terms of their distance from the axis; the family of minimal shapes of genus 1 is thus a one-parameter family.
15. For equilibrium genus 2 surfaces that are not absolute minima of the elastic curvature energy E, there exist at least two orthogonal symmetry planes, which reduces the degeneracy of E [see (*7, 14*)].
16. J. F. Faucon, M. D. Mitov, P. Méléard, I. Bivas, P. Bothorel, *J. Phys. (Paris)* **50**, 2389 (1989); X. Michalet, B. Fourcade, D. Bensimon, *Phys. Rev. Lett.* **72**, 168 (1994).
17. SURFACE EVOLVER is a public domain program written by K. Brakke [*Exp. Math.* **1**, 141 (1992)].
18. The phospholipids used were mostly DMPC (dimyristoylphosphatidylcholine) and $DC_{8,9}PC$ [1,2-*bis*(10,12-tricosadinoyl)-*sn*-glycero-3-phosphatidylcholine] obtained in crystal powder form (Avanti Polar Lipids, Alabaster, AL). We prepared vesicles by hydration of a small amount of crystal, following a procedure described in (*12*).
19. We used a phase-contrast optical microscope (Nikon, Diaphot) coupled to a charge-coupled device camera (Sony). Pictures, which show a "cut" (that is, roughly the contour) of the vesicles in the focal plane, are recorded on video tape or further analyzed on a personal computer. The size of the vesicles is on the order of 10 μm, and their topology is determined by comparison of their different contours (which can be successively observed on a time scale of some minutes because of the slow Brownian rotation of the vesicles) to numerical models of genus 2 surfaces calculated with the SURFACE EVOLVER program (*17*).

20. We thank F. Jülicher, U. Seifert, and R. Lipowsky for stimulating discussions, V. Croquette for help with the digital processing of the pictures, and K. Brakke for the use of SURFACE EVOLVER.

24 February 1995; accepted 26 May 1995

Two-Dimensional Imaging of Potential Waves in Electrochemical Systems by Surface Plasmon Microscopy

Georg Flätgen, Katharina Krischer,* Bruno Pettinger, Karl Doblhofer, Heinz Junkes, Gerhard Ertl

The potential dependence of resonance conditions for the excitation of surface plasmons was exploited to obtain two-dimensional images of the potential distribution of an electrode with high temporal resolution. This method allows the study of spatiotemporal patterns in electrochemical systems. Potential waves traveling across the electrode with a speed on the order of meters per second were observed in the bistable regime of an oscillatory electrochemical reaction. This velocity is close to that of excitation waves in nerve fibers and is far greater than the velocity of reaction-diffusion waves observed in other chemical systems.

All disciplines of science exhibit the phenomenon of spontaneous formation of spatiotemporal patterns from an originally homogeneous state (*1*). In chemical systems, spatial patterns may develop if an autocatalytic reaction is coupled to diffusion of the reacting species. These systems can be described by reaction-diffusion equations and have been intensively investigated (*2*). However, diffusion is not the only mechanism by which information can be passed on. For example, in nerve fibers, excitation states propagate as a result of electric transport phenomena. This is also true in electrochemical systems, where potential gradients are responsible for communication between different parts of the electrode. The coupling of the electrode kinetics to the bulk electrolyte, which is electroneutral, leads to phenomena that are qualitatively different from those expected in systems that can be described by reaction-diffusion equations (*3*). To date, the investigation of these patterns has been hindered by a lack of suitable experimental techniques. Here, we present images of two-dimensional (2D) potential waves in an electrochemical system. They were obtained with surface plasmon (SP) microscopy, a newly developed method for the study of rapid spatial variations at electrochemical interfaces.

In electrochemical systems, spatial patterns are composed of different voltage drops across the electrode-electrolyte interface

Fritz-Haber-Institut der Max-Planck-Gesellschaft, Faradayweg 4-6, D-14195 Berlin (Dahlem), Germany.

*To whom correspondence should be addressed.

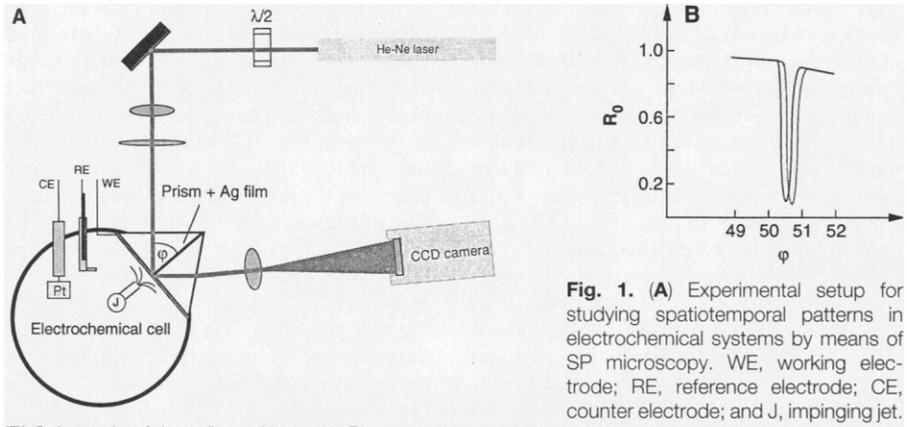

Fig. 1. (**A**) Experimental setup for studying spatiotemporal patterns in electrochemical systems by means of SP microscopy. WE, working electrode; RE, reference electrode; CE, counter electrode; and J, impinging jet. (**B**) Schematic of the reflected intensity R_0 versus the angle of incidence φ at two different values of the potential drop across the electrode-electrolyte interface.

(the so-called double layer) and different concentrations of the adsorbed species that are involved in the reaction. If these species participate in the formation or dissolution of a thick passivating coating, the formation of patterns may become directly visible and can be recorded by means of ordinary light microscopy (*4*), but because these phenomena are no longer strictly 2D, they are usually rather complex mechanistically. Attempts to obtain information about pattern formation at the electrode interface itself have involved measurement of the potential drop across the electrode-electrolyte interface by means of a sequence of aligned microprobes of potential (*5*). However, the applicability of this method is restricted by the screening effects of the probes as well as by low spatial or temporal resolution, or both, in the study of 2D systems. In contrast, SP microscopy probes the electric charge of the electrode, which reflects the potential drop across the electrode-electrolyte interface. This method combines high spatial and temporal resolution with minimal perturbation.

The optical excitation of SPs at metal-electrolyte interfaces and its dependence on applied potential have been studied in some detail (*6*). Limited lateral extension of SPs has been used to study variations in the thickness of Langmuir-Blodgett films (*7*). The combination of these two approaches makes it possible to record patterns made up of variations in potential drops across the electrode-electrolyte interface. In our experimental setup (Fig. 1A), the working electrode consists of a Ag film (50 nm) evaporated onto a glass prism (LASF35, Schott, Mainz, Germany). The electrode is irradiated from behind through the prism by a broadened laser beam (p-polarized light from a He-Ne laser), and the reflected beam is imaged onto a screen and recorded with a charge-coupled device (CCD) camera. As the angle of incidence changes, a sharp resonance peak is observed when the condition of the excitation of SPs is fulfilled (Fig. 1B). This specific angle of excitation is a function of the potential drop across the elec-

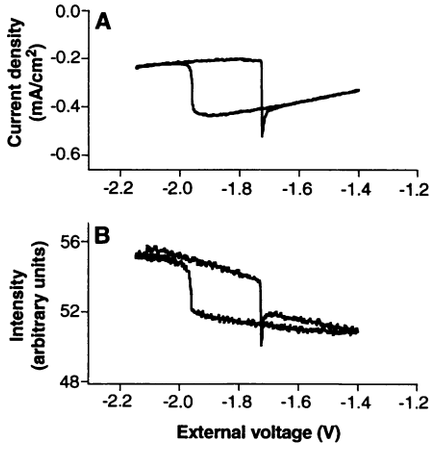

Fig. 2. (**A**) Current-voltage and (**B**) intensity-voltage characteristics of the peroxodisulfate reduction. The voltage is relative to a saturated calomel electrode. The electrolyte (2 mM $Na_2S_2O_8$, 0.05 mM Na_2SO_4, 0.01 mM NaOH, and N_2 saturated) was stirred by an impinging jet.

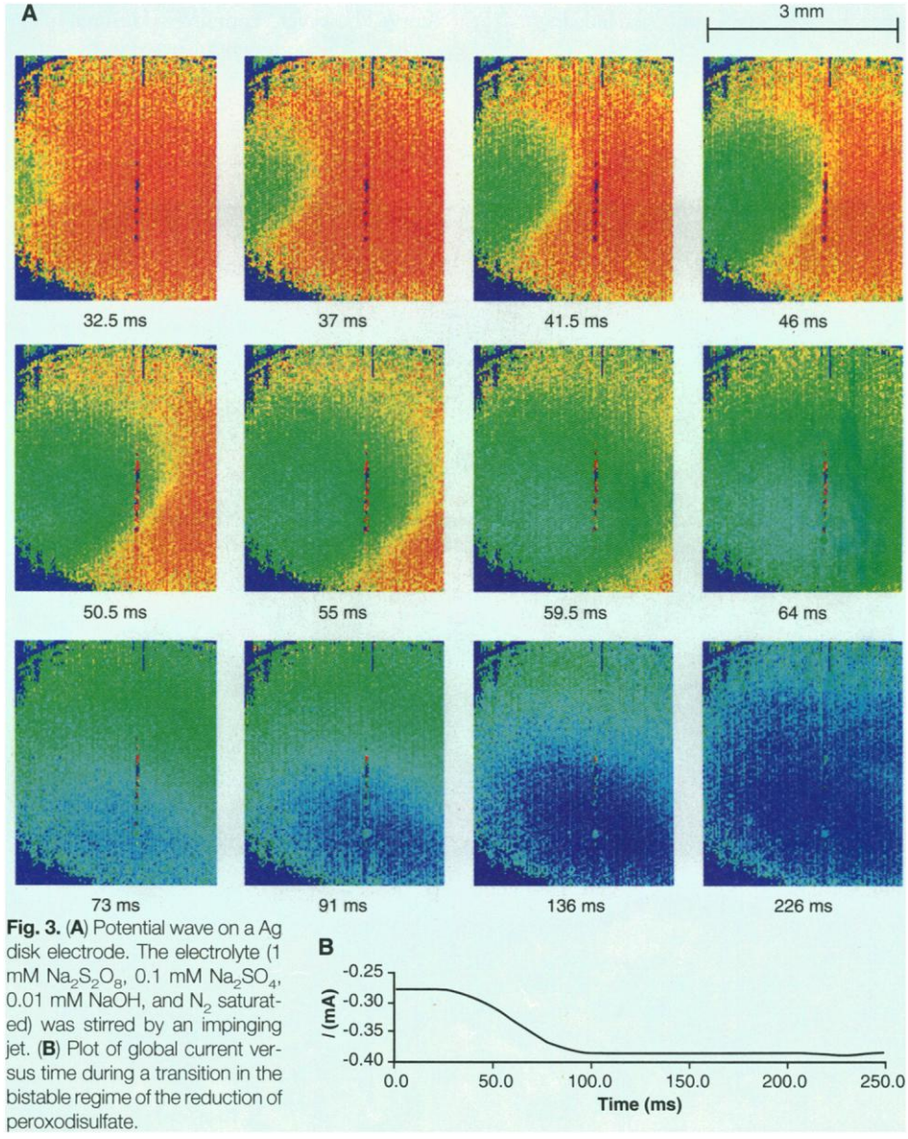

Fig. 3. (**A**) Potential wave on a Ag disk electrode. The electrolyte (1 mM $Na_2S_2O_8$, 0.1 mM Na_2SO_4, 0.01 mM NaOH, and N_2 saturated) was stirred by an impinging jet. (**B**) Plot of global current versus time during a transition in the bistable regime of the reduction of peroxodisulfate.

trode-electrolyte interface. In this application, we kept the angle of incidence fixed (at the maximum slope of the intensity drop) and broadened the laser beam to irradiate the whole electrode. Local variations in the potential drop across the electrode-electrolyte interface result in local variations of the resonance condition of SP excitation and correspondingly in local differences of the intensity of the reflected beam. Imaging the irradiated electrode onto the screen results in an enlarged picture of the potential distribution across the electrode. A temporal resolution of up to 800 frames per second (with 128 by 128 pixels) was achieved with the use of a Dalsa CCD camera with a full-frame transfer architecture, which was connected to an image-processing board. Unlike studies with microprobes, in this setup the electrode was not shielded by any device, and an impinging jet allowed us to define the convection of the electrolyte. Moreover, a perturbation of the temperature, the convective flow, or the potential distribution in the electrolyte by the measurement itself can be excluded.

We examined patterns that developed during the reduction of peroxodisulfate to sulfate under potentiostatic conditions. This reaction is known to exhibit bistability and oscillations in the global current; both instabilities can be traced back to the electrostatic interaction between the peroxodisulfate ions and the electrode (*8*). In the bistable regime, two current densities (called active and passive) exist for a given value of the externally applied voltage (Fig. 2A). This voltage is composed of the potential drop across the electrode-electrolyte interface (ϕ) and the ohmic potential drop (IR drop, where I is the current and R is the resistance) in the electrolyte. Hence, the two states in the bistable regime are characterized by different potential drops across the electrode-electrolyte interface, which in turn correspond to different resonance conditions for SP excitation, as can be seen in the plot of global intensity versus voltage (Fig. 2B). The dependencies of current and intensity on the externally applied voltage look alike because changes in the current always correspond to changes in the voltage drop. The intensity curve, however, contains additional information. In the potential range from –1.4 to –1.7 V, the same current densities were measured during the anodic and cathodic scan, whereas the intensity curve exhibited a small hysteresis. This hysteresis is likely attributable to chemisorption of a species, which also changes the resonance condition (*9*).

We next investigated the breaking of spatial symmetry during the transition from the passive to the active state at a fixed potential. The time trace of the current during a passive-active transition is shown in Fig. 3B. This transition occurs within about 50 ms. In a sequence of images of the disk electrode during this transition (Fig. 3A), the measured intensities were normalized at each point and plotted in a pseudocolor representation. The first image shows the electrode at the beginning of the transition: A small nucleus of the active state is formed at the left edge of the electrode in the otherwise spatially homogeneous passive state. During the transition, this nucleus expands until the entire electrode reaches high current density. The sequence shows that our method not only allows monitoring of a potential wave as it travels across the electrode surface during the passive-active transition, but also reveals some slower spatial alterations that are not connected with any noticeable change in the global current density (see the last four images in Fig. 3A). We attribute these changes to the chemisorption of a species from the solution on a slower time scale. In repetitions of the experiment, the potential waves always originated at different locations on the rim of the electrode, whereas the "chemisorption wave" always originated at the same place. This wave is probably a phase wave that originates from small inhomogeneities of the Ag film. This observation demonstrates a further application of SP microscopy, namely the detection of concentration patterns of chemisorbed particles.

On Ag ring electrodes, potential waves have been observed with microprobes (*3*). For comparison, we conducted the same experiment with a ring-shaped Ag film evaporated onto the prism. The observed time trace (Fig. 4B) again displays a transition from low to high current density. At the beginning, the electrode is in the spatially homogeneous passive state. As with the Ag disk electrode, a nucleus of the active state is formed, and from this nucleus the potential wave spreads over the ring until the whole electrode area is covered (Fig. 4A). These observations are in agreement with the previous results (*3*) and confirm the interpretation presented here.

We have demonstrated that SP microscopy allows the observation of 2D electrochemical potential waves. The strengths of the method are its ability to record the entire surface simultaneously with high temporal resolution (about 1 ms), its nonperturbing nature, its surface specificity, and the accessibility of the electrode, which

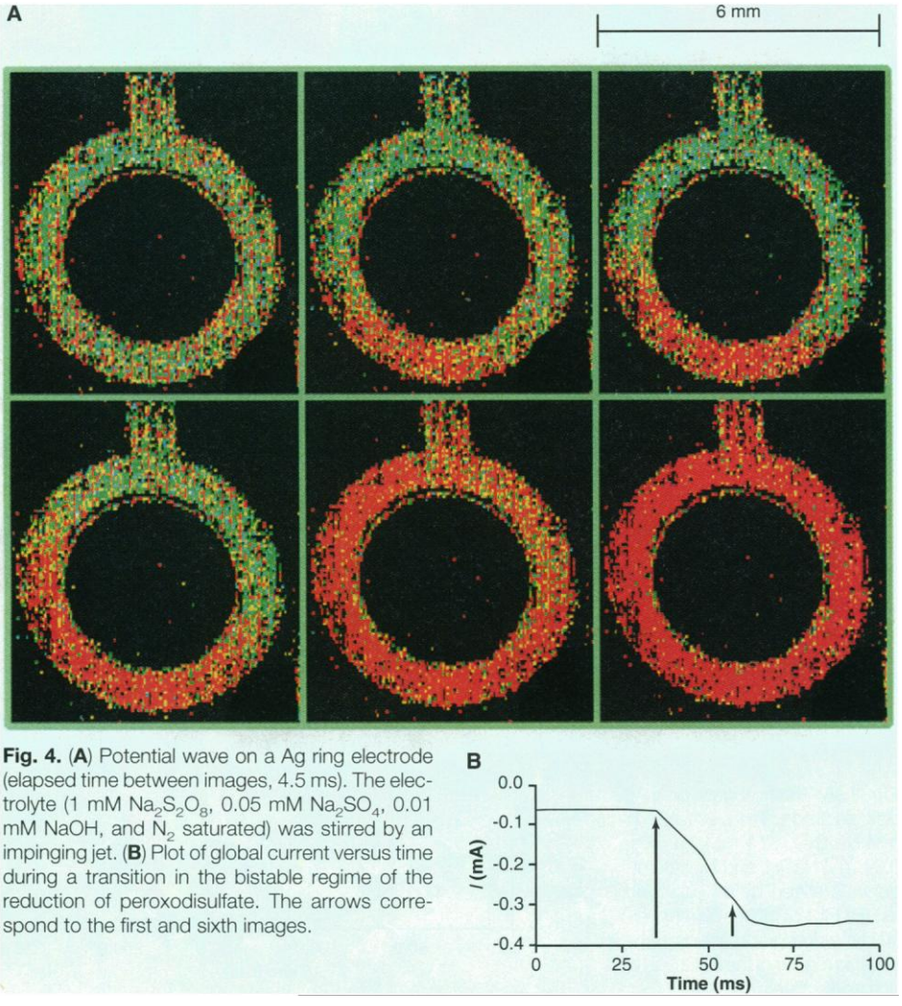

Fig. 4. (**A**) Potential wave on a Ag ring electrode (elapsed time between images, 4.5 ms). The electrolyte (1 mM $Na_2S_2O_8$, 0.05 mM Na_2SO_4, 0.01 mM NaOH, and N_2 saturated) was stirred by an impinging jet. (**B**) Plot of global current versus time during a transition in the bistable regime of the reduction of peroxodisulfate. The arrows correspond to the first and sixth images.

permits a defined convection. This method opens new avenues toward an understanding of spatiotemporal pattern formation in electrochemical systems.

REFERENCES AND NOTES

1. H. Haken, *Synergetics* (Springer-Verlag, Berlin, 1977).
2. A. S. Mikhailov, *Foundations of Synergetics I* (Springer-Verlag, Berlin, 1990).
3. G. Flätgen and K. Krischer, *Phys. Rev. E* **51**, 3997 (1995).
4. J. L. Hudson and M. Basset, *Rev. Chem. Eng.* **7**, 109 (1991); J. L. Hudson, J. Tabora, K. Krischer, I. G. Kevrekidis, *Phys. Lett. A* **179**, 355 (1993); R. D. Otterstedt, N. I. Jaeger, P. J. Plath, *Int. J. Bifurcation and Chaos* **4**, 1265 (1994).
5. K. F. Bonhoeffer, *Z. Elektrochem.* **47**, 147 (1941); O. Lev, M. Sheintuch, L. M. Pisemen, Ch. Yarnitzky, *Nature* **336**, 458 (1988).
6. J. G. Gordon and S. Ernst, *Surf. Sci.* **101**, 499 (1980); D. M. Kolb, in *Surface Polaritons: Electromagnetic Waves at Surfaces and Interfaces*, V. M. Agranovich and D. L. Mills, Eds. (North-Holland, Amsterdam, 1982), pp. 299–329; A. Tadjeddine, *Electrochim. Acta* **34**, 29 (1989).
7. B. Rothenhäusler and W. Knoll, *Nature* **332**, 615 (1988).
8. A. Frumkin, *Z. Elektrochem.* **59**, 807 (1955); W. Wolf, J. Ye, M. Purgand, M. Eiswirth, K. Doblhofer, *Ber. Bunsenges. Phys. Chem.* **96**, 1797 (1992).
9. P. G. Dzhavakhidze, A. A. Kornyshev, A. Tadjeddine, M. I. Urbakh, *Electrochim. Acta* **34**, 1677 (1989); D. M. Kolb, *J. Phys. (Paris)* **38**, C5-167 (1977). A. Tadjeddine, *J. Electroanal. Chem.* **169**, 129 (1984); F. Chao, M. Costa, A. Tadjeddine, *J. Phys. (Paris)* **38**, C5-97 (1977).

10. We thank S. Herminghaus for fruitful discussions and useful suggestions concerning the experimental setup and K. Grabitz for preparing the Ag films. K.K. received support through the Deutsche Forschungsgemeinschaft.

22 February 1995; accepted 15 May 1995

Detection of Creatinine by a Designed Receptor

T. W. Bell,*† Z. Hou, Y. Luo, M. G. B. Drew, E. Chapoteau, B. P. Czech, A. Kumar

An artificial receptor has been designed to bind creatinine with a color change (chromogenic response) caused by proton transfer from one end of the receptor to the other. The receptor was synthesized and found to extract creatinine from water into chlorocarbon solvents. The color change in the organic layer is specific for creatinine relative to other organic solutes, and it is selective for creatinine relative to sodium, potassium, and ammonium ions. The chromogenic mechanism is revealed by x-ray crystal structures of creatinine, the free receptor, and the complex, showing "induced fit" binding resulting from electronic complementarity between host and guest.

Creatinine (*1*) is an end product of nitrogen metabolism. In healthy individuals, it is transported by the kidneys from blood to urine. Blood levels of urea nitrogen and creatinine are key indicators of renal function (*2*), but current creatinine assays have several shortcomings. The Jaffé reaction, in which a colored product is formed from creatinine and picrate in alkaline solution, remains the prevalent method, despite its poor specificity. During the past two decades, several enzymatic methods have appeared, the most promising of which require four or five enzymes (*3*, *4*). Apparently, these approaches are more specific than the Jaffé method, but they suffer the shortcomings of certain interferences, expense, and limited stability. The work reported here demonstrates that supramolecular chemistry (*5*–*7*) can be applied to the design of chromogenic reagents for detection of clinically important molecules.

T. W. Bell, Z. Hou, Y. Luo, Department of Chemistry, State University of New York, Stony Brook, NY 11794–3400, USA.
M. G. B. Drew, Department of Chemistry, The University, Whiteknights, Reading, RG6 2AD, UK.
E. Chapoteau, B. P. Czech, A. Kumar, Diagnostics Division, Bayer Corporation, Tarrytown, NY 10591–5097, USA.
*To whom correspondence should be addressed.
†Present address: Department of Chemistry–216, University of Nevada, Reno, NV 89557–0020, USA.

The receptor (**1**, Fig. 1) was designed with the use of Cram's principles (*7*) of host-guest complementarity and host preorganization (*5*–*8*). The successful binding of creatinine (**2**) by three hydrogen bonds was expected to cause the transfer of a proton from the OH group of the receptor to its end nitrogen atom. The resulting complex (**1·2**) would then have a dipolar structure; the delocalization of the negative and positive charges was expected to cause a visible color change. In this designed receptor, the chromogenic group is intrinsic to the preorganized binding site and communicates directly with the bound guest (*9*). In contrast, color-producing or fluorescent moieties generally cannot be incorporated into the binding sites of biomolecular receptors, enzymes, or antibodies without altering their desirable binding characteristics.

As shown in Fig. 2, creatinine receptor **1** was synthesized in five steps (*10*) from intermediate **3** (*11*). The phenol ring in **4** was protected from ozonolysis as ester **5**. Partial hydrolysis of the acetate group occurred during isolation of product **6**, so this intermediate was converted to phenol **8** without purification. Nitration of **8** gave the target receptor (**1**), which was difficult to purify because of its acid-base properties and low solubility in most solvents. Chromogenic analytical reagents are used in very small quantities, so the synthesis outlined in Fig. 2 is effective, despite its

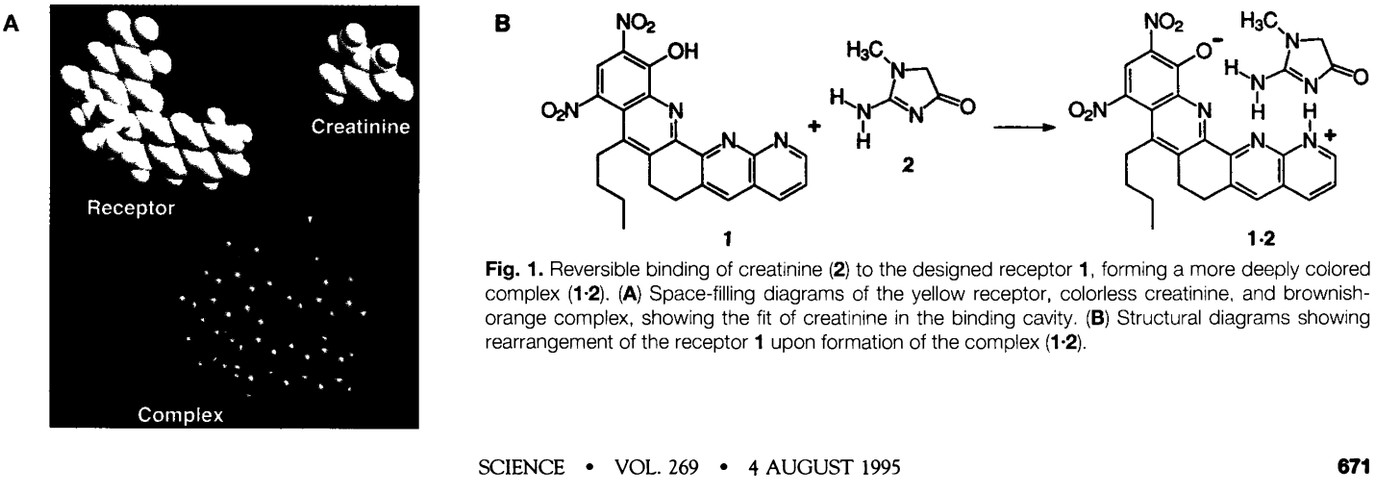

Fig. 1. Reversible binding of creatinine (**2**) to the designed receptor **1**, forming a more deeply colored complex (**1·2**). (**A**) Space-filling diagrams of the yellow receptor, colorless creatinine, and brownish-orange complex, showing the fit of creatinine in the binding cavity. (**B**) Structural diagrams showing rearrangement of the receptor **1** upon formation of the complex (**1·2**).